The mitochondrial calcium uniporter is crucial for the generation of fast cortical network rhythms

– FINAL VERSION –

The mitochondrial calcium uniporter is crucial for the generation of fast cortical network rhythms

Carlos Bas-Orth[1,2,6,a], Justus Schneider[3,6,a], Andrea Lewen[3,6], Jamie McQueen[4,5], Kerstin Hasenpusch-Theil[5], Thomas Theil[5], Giles E. Hardingham[4,5], Hilmar Bading[1,6,b], and Oliver Kann[3,6,b]*

[1] Department of Neurobiology, University of Heidelberg, D-69120 Heidelberg, Germany

[2] Institute of Anatomy and Cell Biology, University of Heidelberg, D-69120 Heidelberg, Germany

[3] Institute of Physiology and Pathophysiology, University of Heidelberg, D-69120 Heidelberg, Germany

[4] UK Dementia Research Institute, University of Edinburgh, Edinburgh EH16 4TJ, United Kingdom

[5] Centre for Discovery Brain Sciences, University of Edinburgh, Edinburgh EH8 9XD, United Kingdom

[6] Interdisciplinary Center for Neurosciences (IZN), University of Heidelberg, D-69120 Heidelberg, Germany

[a,b] These authors contributed equally to this work

* Correspondence to: Dr. Oliver Kann, Institute of Physiology and Pathophysiology, University of Heidelberg, Im Neuenheimer Feld 326, D-69120 Heidelberg, Germany; Phone: 0049.(0)6221.544560
E-mail: oliver.kann@physiologie.uni-heidelberg.de
ORCID iD: https://orcid.org/0000-0003-4365-8067

Funding: This work was supported by the Deutsche Forschungsgemeinschaft (Collaborative Research Center 1134, projects B02 and C03; FOR2289, BA1007/9-1 and BA3679/4-2) and also by the UK Medical Research Council, Alzheimer's Research UK and Alzheimer's Society

Running headline: MCU and fast neuronal rhythms

Abstract

The role of the mitochondrial calcium uniporter (MCU) gene (*Mcu*) in cellular energy homeostasis and the generation of electrical brain rhythms is widely unknown. We investigated this issue in mice and rats using *Mcu*-knockout and -knockdown strategies in vivo and in situ and determined the effects of these genetic manipulations on hippocampal gamma oscillations (30-70 Hz) and sharp wave-ripples. These physiological network states require precise neurotransmission between pyramidal cells and inhibitory interneurons, support spike-timing and synaptic plasticity and are associated with perception, attention and memory. Absence of the MCU resulted in (i) gamma oscillations with decreased power (by >40%) and lower synchrony, including less precise neural action potential generation ('spiking'), (ii) sharp waves with decreased incidence (by about 22%) and decreased fast ripple frequency (by about 3%) and (iii) lack of activity-dependent pyruvate dehydrogenase dephosphorylation. However, compensatory adaptation in gene expression related to mitochondrial function and glucose metabolism was not detected. These data suggest that the neuronal MCU is crucial for the generation of network rhythms, most likely by influences on oxidative phosphorylation and perhaps by controlling cytoplasmic Ca^{2+} homeostasis. This work contributes to an increased understanding of mitochondrial Ca^{2+} uptake in cortical information processing underlying cognition and behaviour.

Keywords

calcium signalling, electrophysiology, mitochondria, neurometabolic coupling, neuronal activity

Abbreviations

AAV, adeno-associated virus; ACSF, artificial cerebrospinal fluid; CMR, cerebral metabolic rate; DIV, days in vitro; GAM, gamma oscillations; KD, knockdown; KO, knockout; LFP, local field potential; MCU, mitochondrial calcium uniporter; *Mcu*, MCU gene; PDH, pyruvate dehydrogenase; PV, parvalbumin; RP; ripple; shRNA, short hairpin RNA; SW, sharp wave

Introduction

The integrative role of mitochondrial Ca^{2+} uptake and cycling in central neurons has been established on molecular, cellular and system levels [1-3]. This role comprises a variety of physiological processes, such as maintenance of intracellular Ca^{2+} homeostasis, synaptic activity, vesicle exocytosis and energy metabolism [4-10]. During neurometabolic coupling, mitochondrial Ca^{2+} can act as a feed-forward regulator of oxidative phosphorylation and ATP production in mitochondria by affecting the activity of pyruvate dehydrogenase (PDH), several TCA cycle enzymes and F_1F_O-ATP synthase [1, 11, 12]. Moreover, the detrimental consequences of excessive mitochondrial Ca^{2+} uptake in neurons have been studied under various pathophysiological conditions [1, 13, 14]. Excessive mitochondrial Ca^{2+} uptake can trigger several harmful events, including opening of the mitochondrial permeability transition pore and loss of mitochondrial membrane potential, which potentially lead to bioenergetic failure and neuronal death [15-19]. Both initiation and cellular consequences of excessive mitochondrial Ca^{2+} uptake likely differ in ischemia, epilepsy and age-related neurodegenerative diseases, however [20-23].

During neuronal activity, cytoplasmic Ca^{2+} transients are associated with the uptake of Ca^{2+} into mitochondria and increased mitochondrial matrix Ca^{2+} concentration [2, 6, 8, 24, 25]. Importantly, mitochondrial Ca^{2+} uptake requires the recently identified mitochondrial Ca^{2+}

uniporter (MCU) [26, 27], which is part of a large protein complex [2, 28]. Alternative routes for mitochondrial Ca^{2+} uptake, such as ion exchangers and the rapid uptake mode, have been also described [2, 29, 30].

The role of the MCU in the cellular homeostasis underlying the generation of fast neuronal network rhythms that associate with cortical information processing in vivo is unknown. This role is of particular interest because the awake human brain features *per se* a high metabolic rate that further increases during functional activation of primary cortical regions, with mean values of 27 ± 10% and 20 ± 13% for ΔCMR_{glc} and ΔCMR_{O2}, respectively [31-33]. Therefore, active neurons critically depend on efficient neurometabolic coupling and high performance of mitochondrial oxidative phosphorylation [22, 31]. In theory, such neurometabolic coupling can be achieved both by cytosolic Ca^{2+} that stimulates mitochondrial substrate carriers and by mitochondrial matrix Ca^{2+} that stimulates TCA cycle dehydrogenases. However, whether mitochondrial Ca^{2+}-uptake via the MCU complex is required to support physiological neuronal network activity by regulating cellular energy metabolism and/or Ca^{2+} homeostasis is widely unknown [2].

We started to address this by studying gamma oscillations (30-70 Hz) and sharp wave-ripples in hippocampal slice preparations [34-37]. These physiological network rhythms require precise synaptic transmission between excitatory pyramidal cells and inhibitory

interneurons and occur during wakefulness and sleep [38, 39]. They support, for example, spike-timing and synaptic plasticity on the cellular level and are thus thought to contribute to the emergence of higher brain functions, such as perception, attention and memory [38-40]. We used various knockout (KO) and knockdown (KD) strategies of the *Mcu* in vivo and in situ.

Materials and methods

Mcu-knockout and Mcu-knockdown strategies

All animal experiments conformed to national and institutional guidelines including the Animals [Scientific Procedures Act] 1986 (UK), and the Council Directive 2010/63/EU of the European Parliament, and had full Home Office ethical approval (University of Edinburgh Animal Welfare and Ethical Review Body; University of Heidelberg Animal Welfare Office and Regierungspraesidium Karlsruhe, licenses T46/14 and T96/15). All animals were maintained in pathogen-free and light- (12hr light/ 12hr dark) and temperature-controlled (22 °C ± 2 °C) conditions. Food (LasVendi Rod 16 or Rod 18) and water were available *ad libitum.* Animals were group-housed in conventional cages with ABBEDD LT-E-001 bedding material and were provided with environmental enrichment.

Animal welfare was assessed daily by staff of the animal facility. Experiments were performed and reported in accordance with the ARRIVE guidelines. The investigator was blinded for the genotype.

To obtain mice with brain-specific loss of *Mcu* expression, *Mcu*$^{fl/fl}$ mice (colony name: B6N-Atm1Brd-Mcu$^{tm1c(EUCOMM)Hmgu/H}$ MGI Allele name: Mcu$^{tm1c(EUCOMM)Hmgu}$, MGI ID: 5692853, EMMA ID: EM:10448) were crossed with C57BL/6 Emx1-Cre mice [41] in which the neo cassette had been removed by crossing with the ROSA26Fki Flp deleter mice [42]. *Mcu*$^{fl/fl}$ mice were generated by MRC Harwell from targeted ES cells made by The European Conditional Mouse Mutagenesis Program, as part of the International Mouse Phenotyping Program. Intercrosses of *Mcu*/*Cre*$^{+}$ double heterozygotes with heterozygous *Mcu*/*Cre*$^{-}$ mice were carried out to generate experimental *Mcu* knockout (*Mcu*/*Cre*$^{+}$) and wildtype controls (Wt/*Cre*$^{+}$). Animals were genotyped by PCR using the following primers (5'-3'): A: CCCAGGCCCATGGTTGATTT, B: GCACCTGCAACACTATAAACATTCAA; C GTGCAGGTCTATACTTACACACAAAGGACA, D: GAGCTGTGTCTGCACCTGCAACA; Primer pair A-B recognized the wild-type allele and primer pair C-D recognized the KO allele. Cre was genotyped using the following

primers (5’-3’) F: GAACCTGATGACATGTTCAGG, R: AGTGCGTTCGAACGCTAGAGCCTGT.

Recombinant adeno-associated viral vectors for the expression of short hairpin RNAs (shRNAs) contain a ubiquitous U6 promoter for shRNA expression and a CaMKII promoter driving mCherry expression. Note that due to the use of a CaMKII promoter the fluorescent infection marker is expressed in glutamatergic neurons only, while shRNAs are expressed in all infected cells. To verify that serotype 1/2 efficiently targets parvalbumin-expressing GABAergic basket cells, we infected slice cultures with an rAAV that expresses mCherry under the control of a ubiquitous CMV promoter. Immunostaining for parvalbumin confirmed reliable infection of basket cells (Suppl. Fig. 2). The following shRNA target sequences were used in this study (5′–3′): control shRNA targeting LacZ: CCAACGTGACCTATCCCATTA, *Mcu* shRNA-1: TAGGGAATAAAGGGATCTTAA [18], *Mcu* shRNA-2: ATGACGCGCCAGGAATATG, *Mcu* shRNA-3: GGGCTTAGCGAGTCTTGTC [18]. Viral particles were produced as described [43]. Slice cultures were infected with rAAVs on DIV 4-5 by careful application of 1 µl virus solution onto each slice.

Slice preparations

Wild type and *Mcu*-KO male mice (6-12 weeks old) were anaesthetised with CO_2 and decapitated. The brain was quickly removed and maintained in cooled (4°C) artificial cerebrospinal fluid (ACSF), saturated with 95% O_2 and 5% CO_2. After removal of frontal brain structures and the cerebellum, horizontal entorhinal-hippocampal slices (400 µm) were prepared using a vibratome (VT 1000s, Leica, Bensheim, Germany). These acute slices were stored in a Haas-type interface chamber at 34 ± 1°C for recovery of at least 2 hours as well as for experimental recordings. Slices with incomplete entorhinal-hippocampal structures were excluded.

Slice cultures were prepared as described [36, 44]. In brief, hippocampal slices (400 µm) were cut with a McIlwain tissue chopper (Mickle Laboratory Engineering Company Ltd., Guildford, UK) from 10 day-old male Wistar rats under sterile conditions. Slices with intact hippocampal structures were maintained on Biopore™ membranes (Millicell standing inserts, Merck Millipore, Darmstadt, Germany) between culture medium, which consisted of 50% minimal essential medium, 25% Hank's balanced salt solution (Sigma-Aldrich, Taufkirchen, Germany), 25% heat-inactivated horse serum (Life Technologies, Darmstadt, Germany), and 2 mM L-glutamine (Life Technologies) at pH 7.3 titrated with

Trisbase, and humidified normal atmosphere (5% CO_2, 36.5°C) in an incubator (Heracell, Thermoscientific, Dreieich, Germany). Slices were randomly assigned to experimental groups. The culture medium (1 ml) was replaced three times per week. Slice cultures were used after 7-14 days in vitro (DIV), when the tissue had recovered from slice preparation and damaged cut surfaces had been re-organized [1, 45].

Recording solutions and drugs

Acute slices and slice cultures were stored in a Haas-type interface chamber and constantly supplied with heated (34 ± 1°C) recording solution, i.e. ACSF containing: 129 mM NaCl, 3 mM KCl, 1.25 mM NaH_2PO_4, 1.8 mM $MgSO_4$, 1.6 mM $CaCl_2$, 26 mM $NaHCO_3$, and 10 mM glucose [36, 44]. The pH was 7.3 when the recording solution was saturated with 95% O_2 and 5% CO_2. The gas supply to the interface chamber was 1.5 l/min (95% O_2 and 5% CO_2).

Gamma oscillations were induced by bath application of acetylcholine (2 µM) and physostigmine (400 nM) in rat slice cultures or the muscarinic receptor agonist carbachol (5 µM) in mouse acute slices [34, 36, 45, 46].

Carbachol and physostigmine were purchased from Tocris (R&D Systems GmbH, Wiesbaden-Nordenstadt, Germany). Standard salts and acetylcholine were from Sigma-Aldrich (Taufkirchen, Germany).

Recordings of local field potentials

In rat slice cultures the local field potential was recorded with glass electrodes (tip diameter 3-5 µm) that were pulled from GB150F-8P borosilicate filaments (Science Products GmbH, Hofheim, Germany) with a PC-10 vertical micropipette puller (Narishige International Ltd., London, UK) and backfilled with ACSF. In mouse acute slices carbon fibre electrodes (Kation Scientific, Minneapolis, MN, USA) were used. The microelectrodes were positioned in stratum pyramidale of the CA3 region with a mechanical micromanipulator (MX-4, Narishige). Extracellular field potentials were low-pass filtered at 3 kHz, and digitised at 10 kHz using CED 1401 interface and processed with Spike2 software (Cambridge Electronic Design, Cambridge, UK) for offline analysis.

Offline signal analysis of 5 min data segments from local field potential recordings was performed using custom-made scripts in MATLAB 2015a (The MathWorks, Inc., Natick, MA, USA). Recordings of gamma oscillations were low-pass filtered with a digital

Butterworth algorithm at 200 Hz cutoff frequency and processed with Welch's algorithm and fast Fourier transform with a Hamming window size of 32768 points for calculation of the power spectral density (power) (bin size of 0.3052 Hz). Gamma oscillations were analysed for peak power, frequency and full width at half-maximum (FWHM). Recordings of sharp wave-ripples were band-pass filtered with a Butterworth algorithm between 5-60 Hz corner frequencies to detect the transient sharp wave component. Amplitude and incidence of sharp waves were measured and averaged. Ripples superimposed on the sharp wave were analysed using continuous wavelet transformation. Multi-unit activity was assessed by high-pass filtering of the local field potential with a Butterworth algorithm at 700 Hz corner frequency. The threshold for unit detection was set to 4.5 standard deviations of the local field potential during spontaneous asynchronous activity and the correctness of unit detection was checked visually.

Toluidine blue staining and immunohistochemistry

For toluidine blue staining (Sigma-Aldrich), acute hippocampal slices were fixed overnight with 4% paraformaldehyde in phosphate-buffered salt solution (PBS), incubated for 5 h in 30% sucrose (AppliChem GmbH, Darmstadt, Germany) and cut in thin sections (40 µm)

with a CM1850 cryostat (Leica Microsystems GmbH, Nussloch, Germany). Sections were mounted on slides, exposed to descending ethanol series, briefly rinsed in double-distilled water and then incubated in 0.1% toluidine blue working solution (pH 2.3) for 1-5 min. Thereafter, the sections were briefly rinsed in double-distilled water. 95% ethanol with traces of glacial acetic acid was used for colour differentiation of the staining. The sections were then exposed to ascending ethanol series, a 1:1 mixture of 100% ethanol and xylene, and finally xylene for 6-10 min. Afterwards the sections were embedded with Entellan®Neu (Merck Millipore, Schwalbach, Germany).

For GFP, parvalbumin and GFAP staining mice were anaesthetized by intraperitoneal injection of sodium pentobarbital and transcardially perfused with 20 ml of PB followed by 20 ml of ice cold 4% PFA. A vibratome (Leica, UK) was used to cut 50 µm thick sections which were stored free-floating in PB at 4˚C until use. Sections were washed in PB, blocked with 5% donkey serum for 1 hr and incubated in the following antibodies overnight: anti-GFP conjugated to FITC (1:500 Abcam ab6662), mouse anti-parvalbumin (1:5000, Swant PV235) and rabbit anti-GFAP (1:1000, Dako Z0334). Sections were then washed in PB and incubated in donkey anti-mouse Alexa Fluor 546 antibody (1:500) and donkey anti-rabbit Alexa Fluor 546 antibody (1:500) for 1 hr before being washed and

mounted onto slides. Sections were imaged using a Leica AF6000LX immunofluorescence microscope.

Western blotting

Wild type, *Mcu*/*Cre*$^{-}$ and *Mcu*-KO mice were anaesthetized with isoflurane and decapitated. Brains were quickly removed, the hippocampus dissected and CA3 microdissected using a scalpel blade. The tissue was snap frozen and stored at -80˚C until required. Samples were homogenized in RIPA buffer (50mM Tris-HCl (pH 7.5), 150mM NaCl, 1mM EDTA, 0.1% SDS, 0.5% sodium deoxycholate) containing protease and phosphatase inhibitors (Roche, UK). The samples were then lysed in 1.5x LDS sample buffer (NuPage, Life Technologies) and boiled at 100°C for 10 min. Approximately 10 µg of protein was loaded onto a precast gradient gel (4–16%; Invitrogen) and subjected to electrophoresis. Western blotting onto a PVDF membrane was then performed using the Xcell Surelock system (Invitrogen) according to the manufacturer's instructions. Following the protein transfer, the PVDF membranes were blocked for 1 hr at room temperature with 5% (w/v) non-fat dried milk in TBS with 0.1% Tween-20. The membranes were incubated at 4°C overnight with the primary antibodies diluted in blocking solution: Rabbit anti-

MCU (1:4000, Sigma HPA016480) and rabbit anti-beta actin (1:50000, Abcam ab8227). For visualisation of Western blots, HRP-based secondary antibodies were used followed by chemiluminescent detection on Kodak X-Omat film. Western blots were digitally scanned and densitometric analysis was performed using Image J.

Gene expression analysis

Wild type and *Mcu*-KO mice (6-12 weeks old) were anaesthetised with CO_2 and decapitated. Hippocampal area CA3 was rapidly dissected and flash frozen in liquid nitrogen. RNA was isolated from frozen tissue using an RNeasy Microarray Tissue Mini kit (Qiagen) with additional on-column DNase I digestion according to the manufacturer's instructions. 460ng RNA per sample were used to prepare cDNA using a RT2 First Strand Kit (Qiagen) according to the manufacturer's instructions. Real-time PCR was performed on an ABI StepOnePlus system using RT2 SYBR® Green ROX™ qPCR Mastermix and RT2 Profiler PCR Arrays PAMM-087ZA (mouse mitochondria) and PAMM-006ZA (mouse glucose metabolism). Expression of target genes was normalized against the geometric mean of Actb, Gapdh, and Gusb as endogenous control genes. Heatmaps (Figure 7) were generated with Heatmapper [47].

pPDH analysis

Acute slices were recorded in standard buffer in a recording chamber, or were treated with carbachol in a recording chamber for 40 min. Slices were then fixed overnight with 4% formaldehyde at 4 °C. After keeping the slices in 30% sucrose (AppliChem, Darmstadt, Germany) they were resliced into 50µm sections on a cryotome (CM1850, Leica Microsystems, Wetzlar, Germany). Free floating sections were blocked and permeabilised with 5% normal goat serum and 0.3% Triton X-100 for 90 minutes at RT, then labelled overnight at 4°C with a mixture of primary antibodies (mouse anti-PDH E1-alpha, Life Technologies 456600, lot 456600/G0529, 1:500; rabbit anti-pPDH Ser293, Millipore ABS204, lot 2315725, 1:2,000), and then labelled over night at 4°C with a mixture of secondary antibodies (Alexa 594-labelled goat anti-mouse IgG, Thermo Fisher Scientific A-11005, and Alexa 488-labelled donkey anti-rabbit IgG, Thermo Fisher Scientific R37118; both 1:1,000). Sections were counterstained with Hoechst 33258 (Sigma-Aldrich, 1 µg/ml), and mounted in Mowiol 4-88 (Calbiochem).

Images were recorded in sequential mode on a Leica TCS SP8 confocal microscope equipped with a Leica HC PL APO CS2 63x NA 1.4 oil-immersion objective (pixel size

240nm x 240nm). Images were imported into FIJI [48] and converted to 32-bit. 488 nm and 552 nm excitation channels were split and a threshold was set in both channels to contrast mitochondria. The 488 nm excitation channel (pPDH) was divided by the 552 nm excitation channel (total PDH). The resulting 488 nm/552 nm ratio image was displayed in fire lookup table. The 488 nm/552 nm ratio was measured in stratum pyramidale (as identified in the Hoechst channel) and data were exported to Microsoft Excel. Image acquisition and data analysis were done blind to genotype.

Calculations and statistics

Electrophysiological data are presented as median with 25th and 75th percentile derived from 'n' acute slices (cultured slices) from 'N' mice (rats), unless stated otherwise. Statistical significance, $P < 0.05$ or confidence interval (CI) was determined using SigmaPlot 12.5 (Systat Software, San Jose, CA) and GraphPad Prism (GraphPad Software Inc., La Jolla, USA). Data distribution was checked for normality with Shapiro-Wilk test. Comparisons among paired data were made with Wilcoxon signed-rank test. Comparisons among unpaired data were made with Kruskal-Wallis ANOVA on ranks followed by Dunn's post hoc test. Figures were generated with MATLAB 2015a (MathWorks), and

CorelDRAW (Corel Corporation, Ottawa, Ontario, Canada). Quantitative immunofluorescence data are presented as mean + 95% CI. Data distribution was checked for normality with Shapiro-Wilk test and P value was determined by unpaired two-tailed student's t-test using GraphPad Prism (GraphPad Software Inc., La Jolla, USA).

Results

We used a combined experimental approach to determine the role of the MCU in the generation of fast neuronal network rhythms in the hippocampus of mice and rats.

First, we used acute hippocampal slices from conditional *Mcu*-KO mice. These mice were generated by crossing a floxed *Mcu* mouse line to *Emx1-Cre* mice that express Cre-recombinase in cortical glutamatergic neurons [41]. Notably, in these mice the MCU is still present in GABAergic interneurons, such as parvalbumin-positive, fast-spiking inhibitory interneurons important for the generation of gamma oscillations and sharp wave-ripples [34, 41, 49, 50]. The *Mcu*-KO mice showed no gross differences in the hippocampal cytoarchitecture (Fig. 1 A and B). Western blotting of extracts from the hippocampal CA3 molecular layer confirmed significant knockout of MCU (Fig. 1 C and D) as compared to wild type and *Mcu*/*Cre*$^{-}$ mice. To confirm the distribution and identity of *Emx1-Cre*

expressing cells, *Emx1-Cre* mice were crossed with B6;129S4-Gt(ROSA)26Sor$^{tm9(EGFP/Rpl10a)Amc}$/J mice, in which Cre-mediated excision results in eGFP expression. This revealed expression in neurons throughout the cortex and hippocampus, consistent with previous studies [41] (Fig. S1 A and B). Immunohistochemistry confirmed the lack of GFAP (astrocyte marker) and parvalbumin (interneuron marker) co-expression with eGFP (Fig. S1 C-J).

As a second approach, we used organotypic hippocamal slice cultures from rats [36, 44]. In these slice cultures, *Mcu* was knocked down by recombinant adeno-associated virus-mediated expression of *Mcu*-directed short hairpin RNAs (shRNAs) in excitatory and inhibitory neurons [18] (Suppl. Fig. 2).

In these slice preparations (Fig. 1 E), we performed local field potential recordings, including fast Fourier transform, to characterize the properties of cholinergically-induced, persistent gamma oscillations and spontaneously-occurring, recurrent sharp wave-ripples, both of which share many features with their counterparts in vivo [36, 37, 46, 51]. We focussed on the CA3 region, which is an intrinsic generator of gamma oscillations and sharp wave-ripples in the hippocampus [34, 50, 51], and shows a higher *Mcu*-expression of about 2-fold compared with the CA1 region [52].

Disturbances of gamma oscillations

Gamma oscillations with a frequency of around 32 Hz were present in the CA3 region of wild type and *Mcu*-KO mice (Fig. 2 A, B and D). However, *Mcu*-KO mice showed a strong decrease in the power of gamma oscillations by about 87% (Fig. 2 C) as well as an increase in full width at half maximum (FWHM), reflecting less precision (Fig. 2 E). We note that the oscillation power increases with number and synchrony of postsynaptic currents at gamma-frequency, whereas FWHM increases with jitter in the timing of postsynaptic currents [37].

Similar disturbances in the power of gamma oscillations were present in the CA3 region of rat slice cultures expressing shRNAs against *Mcu*. To obtain robust results, we used three different shRNA sequences. Expression of sh1 and sh2 resulted in a decrease in the power of gamma oscillations by about 40.9% and 65.9%, respectively (Fig. 3 A-G). The increase in FWHM was only present in slice cultures expressing sh2 and was accompanied by an increase in gamma oscillation frequency (Fig. 3 H and I). By contrast, expression of sh3 resulted in a decrease in FWHM (Fig. 3 G-I). Thus, we broadly confirm our findings in *Mcu*-KO mice with two out of three variants of shRNAs in rat slice cultures.

These findings suggest that the MCU is required for proper generation of gamma oscillations.

Disturbances of neuronal spiking synchronization

We further characterized the synchronization of neuronal action potential generation ('spiking') during gamma oscillations. For this purpose, multi-unit activity was extracted from local field potential recordings (Fig. 4 A). In wild type mice, there was a second peak of the multi-unit intervals present at 20-30 ms, reflecting synchronized neuronal spiking at the gamma-band rhythm (Fig. 4 B). Notably, this second peak of multi-unit intervals was absent in *Mcu*-KO mice. In addition, the timing of multi-unit activity was less concentrated at the negative peak of the gamma-band cycle in *Mcu*-KO mice and thus less precise (Fig. 4 C). The frequency of multi-unit activity was similar in wild type and *Mcu*-KO mice (Fig. 4 D), excluding an overall decrease in neuronal excitability in the mutant.

These findings suggest that the MCU is required for proper synchronization of neuronal spiking during gamma oscillations.

Disturbances of sharp wave-ripples

To test whether the disturbances on the network and cellular level described above are specific for gamma oscillations, we additionally characterized the properties of sharp wave-ripples. Recurrent sharp wave-ripples were present in the CA3 region of wild type and *Mcu*-KO mice (Fig. 5 A). Whereas the amplitude of sharp waves was similar in wild type and *Mcu*-KO mice (Fig. 5 B), the incidence of sharp waves decreased by about 22% in *Mcu*-KO mice (Fig. 5 C). The frequency of fast ripples (Fig. 5 D) decreased by about 3%, and also the number of ripples per sharp wave (Fig. 5 E) was lower in *Mcu*-KO mice.

These findings suggest that the MCU is also required for proper generation of sharp wave-ripples.

Alterations of neurometabolic coupling

Cortical information processing depends on ATP supply by neuronal mitochondria [22]. We therefore reasoned that impaired Ca^{2+}-mediated activation of mitochondrial oxidative metabolism might be one mechanism that underlies the disturbances in neuronal network oscillations in *Mcu*-KO mice. To assess neurometabolic coupling in wild type and *Mcu*-KO mice, we measured activity-dependent PDH dephosphorylation, which is an indicator

of mitochondrial TCA cycle stimulation [11], after 40 minutes of gamma oscillations in acute hippocampal slices (Fig. 6). In slices from wild type mice, PDH phosphorylation was markedly reduced. In contrast, PDH phosphorylation was unchanged in slices from *Mcu*-KO mice.

These findings indicate that during gamma oscillations the Ca^{2+}-dependent stimulation of the mitochondrial TCA cycle is dysfunctional in *Mcu*-KO mice.

Absence of adaptations in gene expression

We next asked if the reduced capability to activate mitochondrial oxidative phosphorylation in *Mcu*-KO mice results in compensatory changes in the expression of metabolic genes. For this purpose, we isolated the CA3 region from hippocampus of control and *Mcu*-KO mice, and analysed mRNA expression of a panel of 168 genes that are related to mitochondrial function or glucose metabolism using RT2 Profiler PCR Arrays (Fig. 7, Suppl. tables 1 and 2). Using a threshold of 2-fold up- or downregulation to identify differentially expressed genes, we found no difference between WT and KO mice in any of the analysed genes.

These findings suggest that under basal conditions there are no compensatory adaptations in energy metabolism in *Mcu*-KO mice, at least at the transcriptional level.

Discussion

Mcu-KO and Mcu-KD strategies

In this study, we used two complementary approaches to investigate the role of the MCU during fast neuronal network rhythms. First, we generated a brain-specific *Mcu*-KO mouse line that lacks expression of the MCU in excitatory cortical and hippocampal neurons. The specific advantage of this approach is the complete lack of MCU expression in targeted neurons, and normal expression elsewhere. However, Emx1 promoter-driven expression of Cre recombinase starts early during development, which potentially allows for compensatory adaptations to occur. In addition, the Emx1 promoter does not drive expression of Cre recombinase in parvalbumin-positive GABAergic interneurons that are important for the generation of fast network oscillations. In a second approach, we therefore used recombinant adeno-associated viruses of serotype 1/2 to express shRNAs against *Mcu* in both excitatory and inhibitory neurons in rat organotypic hippocampal slice cultures (Suppl. Fig. 2). Compared to acute hippocampal slices, the use of organotypic

cultures provides the advantage of better tissue recovery from brain isolation and slice preparation. In addition, the transient knock-down of *Mcu*, albeit less efficient than the genetic knock-out, provides less time for compensatory cellular adaptions to develop. Although all three shRNAs were able to reduce MCU protein levels in rat neurons (Suppl. Fig 3), only two shRNAs were able to phenocopy the mouse knock-out. The reason for the different results obtained with the third shRNA is not clear, but might involve unidentified off-target effects of the third shRNA. However, this observation is not uncommon and, in fact, underscores the importance of using multiple shRNA sequences and additional complementary approaches [53]. Together, using ex vivo slices and slice cultures from the mouse and the rat hippocampus, we conclude that the MCU is required for neurometabolic coupling and generation of proper fast neuronal network rhythms.

Disturbances of gamma oscillations and sharp wave-ripples

The role of the MCU complex in neurometabolic coupling has been addressed in a number of previous experimental studies. These studies, however, focused on widely undefined activation stages of cultured neurons using artificial stimuli [54] or on intense metabolic stress during hypoxic-ischemic brain injury [55].

Here, we used gamma oscillations and sharp wave-ripples as models of physiological neuronal network rhythms. Gamma oscillations emerge in many cortical areas in awake mammals, including humans and have been associated with sensory perception, attentional selection, motor activity and memory formation [22, 39]. Sharp wave-ripples arise in the hippocampus during waking immobility, consummatory behaviour and slow-wave sleep. They assist in transferring compressed hippocampal information to distributed neocortical circuits to support memory consolidation [38, 39]. In addition, sharp wave-ripples have been implicated in erasure of hippocampal memory traces and certain aspects of active spatial navigation [38-40].

Gamma oscillations and sharp wave-ripples rely on the precise synaptic transmission between excitatory pyramidal cells and GABAergic interneurons, in particular parvalbumin-positive, fast-spiking interneurons, such as basket cells [34, 35, 50, 51]. In generating these patterns of activity, pyramidal cells excite fast-spiking inhibitory interneurons that in turn transiently inhibit the perisomatic region of pyramidal cells through rhythmic GABA release. During gamma oscillations, for example, individual pyramidal cells generate action potentials at 1-3 Hz, whereas fast-spiking inhibitory interneurons show much higher firing rates (>20 Hz) [22, 34]. We note that fast-spiking

inhibitory interneurons were not targeted with our *Mcu*-KO strategy, but we nevertheless see a strong phenotype.

We demonstrate disturbances in the generation of gamma oscillations and the underlying neuronal spiking. In addition, we report the lack of activity-dependent PDH dephosphorylation in *Mcu*-KO mice. This indicates that the Ca^{2+}-dependent stimulation of the mitochondrial TCA cycle is impaired, in line with other reports [30, 56] but see [55]. Therefore, our data might primarily reflect an energy deficit in excitatory pyramidal during gamma oscillations that feature high energy expenditure [22, 37]. Similar results have been reported for the skeletal muscle during strenuous work in a different *Mcu*$^{-/-}$ mouse mutant [30]. Since the overall spiking rates were similar in our wild type and *Mcu*-KO mice, the energy deficit might arise in specific subcellular compartments with high energy expenditure, such as glutamatergic presynaptic terminals [57, 58]. This might, for example, result in less precise excitation of fast-spiking inhibitory interneurons through alterations of the synaptic vesicle cycle [10, 22, 59].

However, we also demonstrate disturbances in the generation of sharp wave-ripples that are thought to involve less energy expenditure compared with gamma oscillations [37]. Therefore, the functions of the MCU in excitatory pyramidal cells may not be restricted to neurometabolic coupling and energy metabolism (Fig. 7 E). Similar to other excitable

cells, the MCU also has an important role in Ca^{2+} homeostasis in neurons [2, 60, 61]. During neuronal activity, mitochondrial Ca^{2+} uptake significantly shapes cytoplasmic Ca^{2+} transients and thereby modulates neural excitability [9, 62, 63] and the release of neurotransmitters [4, 7, 59, 64, 65], including nitric oxide [45, 66, 67]. Thus, loss or dysfunction of the MCU might affect neuronal signalling on different levels.

Disturbances of gamma oscillations and sharp wave-ripples might affect spike-timing and synaptic plasticity in local cortical networks as well as information transfer between remote cortical networks [38-40].

Our data suggest that dysfunction of the MCU might result in cognitive impairment, with putative relevance to several neurological and psychiatric disorders [2, 13, 22, 68, 69].

Absence of adaptations in gene expression

Similar to previous studies in different MCU loss-of-function models [30, 55, 56], we found no evidence for impaired cellular function under basal conditions in our newly generated *Mcu*-KO mouse line. As suggested previously [2], these moderate phenotypes might be due to compensatory mechanisms. However, we found no adaptations in gene expression related to mitochondrial functions and glucose metabolism. Therefore, our data support the

notion that stimulation of mitochondrial metabolism by matrix Ca^{2+} is dispensable for basal neuronal function [2]. In fact, recent work has shown that modest stimulation of neurons leading to moderate workloads and moderate increases in cytosolic Ca^{2+} concentration can stimulate mitochondrial ATP production via Ca^{2+}-regulated mitochondrial substrate carriers, such as the Aralar/AGC1 malate-aspartate-shuttle system and SCaMCs (small calcium-binding mitochondrial carriers) [54]. Moreover, mitochondrial oxidative phosphorylation is further regulated by a variety of Ca^{2+}-independent mechanisms, such as the ratios of ADP/ATP, NAD/NADH or CoA/acetyl CoA [70, 71]. Consistent with its high Ca^{2+} concentration threshold for Ca^{2+}-uptake [72, 73], recruitment of the MCU complex for neurometabolic coupling might therefore be especially relevant during neuronal network activity states that feature large increases in intracellular Ca^{2+} and high energy expenditure, such as gamma oscillations.

Conclusions

We provide substantial evidence that the neuronal MCU is crucial for the generation of fast cortical network rhythms, most likely by adapting oxidative phosphorylation, and perhaps by controlling cytoplasmic Ca^{2+} homeostasis. Our study might contribute an increased

understanding of the functions of the MCU during neuronal information processing. Future studies on neuronal Ca^{2+} homeostasis and synaptic transmission as well as on the behavioural level will further clarify these relationships.

Acknowledgements

The authors thank Yan-Wei Tan for providing shRNA against LacZ.

Author contributions

Carlos Bas-Orth: Conceptualization, Funding acquisition, Investigation, Formal analysis, Visualization, Writing – original draft, Writing – review & editing

Justus Schneider: Investigation, Formal analysis, Visualization, Writing – review & editing

Andrea Lewen: Investigation, Formal analysis, Visualization, Writing – review & editing

Jamie McQueen: Resources, Investigation, Formal analysis, Writing – review & editing

Kerstin Hasenpusch-Theil: Resources, Interpretation, Writing – review & editing

Thomas Theil: Resources, Interpretation, Writing – review & editing

Giles E. Hardingham: Conceptualization, Resources, Project administration, Writing – review & editing

Hilmar Bading: Conceptualization, Funding acquisition, Project administration, Writing – review & editing

Oliver Kann: Conceptualization, Funding acquisition, Project administration, Writing – original draft, Writing – review & editing

Declaration of Conflicting Interests

The authors declare that there is no conflict of interest.

Online supplemental material

Three supplementary figures and two supplementary tables are available online.

References

1. Kann O and Kovacs R. Mitochondria and neuronal activity. *Am J Physiol Cell Physiol.* 2007; 292: C641-657. DOI: 10.1152/ajpcell.00222.2006.

2. Llorente-Folch I, Rueda CB, Pardo B, et al. The regulation of neuronal mitochondrial metabolism by calcium. *J Physiol.* 2015; 593: 3447-3462. DOI: 10.1113/JP270254.

3. Kannurpatti SS, Sanganahalli BG, Herman P, et al. Role of mitochondrial calcium uptake homeostasis in resting state fMRI brain networks. *NMR Biomed.* 2015; 28: 1579-1588. DOI: 10.1002/nbm.3421.

4. Billups B and Forsythe ID. Presynaptic mitochondrial calcium sequestration influences transmission at mammalian central synapses. *J Neurosci.* 2002; 22: 5840-5847. DOI: 20026597.

5. Bindokas VP, Lee CC, Colmers WF, et al. Changes in mitochondrial function resulting from synaptic activity in the rat hippocampal slice. *J Neurosci.* 1998; 18: 4570-4587.

6. Duchen MR. Ca(2+)-dependent changes in the mitochondrial energetics in single dissociated mouse sensory neurons. *Biochem J.* 1992; 283 (Pt 1): 41-50.

7. Fluegge D, Moeller LM, Cichy A, et al. Mitochondrial Ca(2+) mobilization is a key element in olfactory signaling. *Nat Neurosci.* 2012; 15: 754-762. DOI: 10.1038/nn.3074.

8. Kann O, Kovacs R and Heinemann U. Metabotropic receptor-mediated Ca2+ signaling elevates mitochondrial Ca2+ and stimulates oxidative metabolism in hippocampal slice cultures. *J Neurophysiol.* 2003; 90: 613-621. DOI: 10.1152/jn.00042.2003.

9. Sanganahalli BG, Herman P, Hyder F, et al. Mitochondrial calcium uptake capacity modulates neocortical excitability. *J Cereb Blood Flow Metab.* 2013; 33: 1115-1126. DOI: 10.1038/jcbfm.2013.61.

10. Rangaraju V, Calloway N and Ryan TA. Activity-driven local ATP synthesis is required for synaptic function. *Cell* 2014; 156: 825-835. DOI: 10.1016/j.cell.2013.12.042.

11. Glancy B and Balaban RS. Role of mitochondrial Ca2+ in the regulation of cellular energetics. *Biochemistry.* 2012; 51: 2959-2973. Review 2012/03/27. DOI: 10.1021/bi2018909.

12. Yellen G. Fueling thought: Management of glycolysis and oxidative phosphorylation in neuronal metabolism. *J Cell Biol.* 2018; 217: 2235-2246. DOI: 10.1083/jcb.201803152.

13. Nicholls DG, Brand MD and Gerencser AA. Mitochondrial bioenergetics and neuronal survival modelled in primary neuronal culture and isolated nerve terminals. *J Bioenerg Biomembr*. 2015; 47: 63-74. DOI: 10.1007/s10863-014-9573-9.

14. Rueda CB, Llorente-Folch I, Traba J, et al. Glutamate excitotoxicity and Ca2+-regulation of respiration: Role of the Ca2+ activated mitochondrial transporters (CaMCs). *Biochim Biophy Acta.* 2016; 1857: 1158-1166. DOI: 10.1016/j.bbabio.2016.04.003.

15. Randall RD and Thayer SA. Glutamate-induced calcium transient triggers delayed calcium overload and neurotoxicity in rat hippocampal neurons. *J Neurosci.* 1992; 12: 1882-1895.

16. Vergun O, Keelan J, Khodorov BI, et al. Glutamate-induced mitochondrial depolarisation and perturbation of calcium homeostasis in cultured rat hippocampal neurones. *J Physiol.* 1999; 519 Pt 2: 451-466.

17. Kovacs R, Schuchmann S, Gabriel S, et al. Free radical-mediated cell damage after experimental status epilepticus in hippocampal slice cultures. *J Neurophysiol.* 2002; 88: 2909-2918. DOI: 10.1152/jn.00149.2002.

18. Qiu J, Tan YW, Hagenston AM, et al. Mitochondrial calcium uniporter Mcu controls excitotoxicity and is transcriptionally repressed by neuroprotective nuclear calcium signals. *Nat Commun.* 2013; 4: 2034.

19. Depp C, Bas-Orth C, Schroeder L, et al. Synaptic Activity Protects Neurons Against Calcium-Mediated Oxidation and Contraction of Mitochondria During Excitotoxicity. *Antioxid Redox Signal.* 2018; 29: 1109-24.

20. Briston T, Selwood DL, Szabadkai G, et al. Mitochondrial Permeability Transition: A Molecular Lesion with Multiple Drug Targets. *Trends Pharmacol Sci.* 2019; 40: 50-70.

21. Dreier JP. The role of spreading depression, spreading depolarization and spreading ischemia in neurological disease. *Nat Med.* 2011; 17: 439-447.

22. Kann O. The interneuron energy hypothesis: Implications for brain disease. *Neurobiol Dis.* 2016; 90: 75-85.

23. Zsurka G and Kunz WS. Mitochondrial dysfunction and seizures: the neuronal energy crisis. *Lancet Neurol.* 2015; 14: 956-966.

24. Kovacs R, Kardos J, Heinemann U, et al. Mitochondrial calcium ion and membrane potential transients follow the pattern of epileptiform discharges in hippocampal slice cultures. *J Neurosci.* 2005; 25: 4260-4269.

25. Kann O, Taubenberger N, Huchzermeyer C, et al. Muscarinic receptor activation determines the effects of store-operated Ca(2+)-entry on excitability and energy metabolism in pyramidal neurons. *Cell Calcium.* 2012; 51: 40-50.

26. Baughman JM, Perocchi F, Girgis HS, et al. Integrative genomics identifies MCU as an essential component of the mitochondrial calcium uniporter. *Nature.* 2011; 476: 341-345.

27. De Stefani D, Raffaello A, Teardo E, et al. A forty-kilodalton protein of the inner membrane is the mitochondrial calcium uniporter. *Nature.* 2011; 476: 336-340.

28. Marchi S and Pinton P. The mitochondrial calcium uniporter complex: molecular components, structure and physiopathological implications. *J Physiol.* 2014; 592: 829-839.

29. Sparagna GC, Gunter KK, Sheu SS, et al. Mitochondrial calcium uptake from physiological-type pulses of calcium. A description of the rapid uptake mode. *J Biol Chem.* 1995; 270: 27510-27515.

30. Pan X, Liu J, Nguyen T, et al. The physiological role of mitochondrial calcium revealed by mice lacking the mitochondrial calcium uniporter. *Nat Cell Biol.* 2013; 15: 1464-72.

31. Erecinska M and Silver IA. Tissue oxygen tension and brain sensitivity to hypoxia. *Respir Physiol.* 2001; 128: 263-276.

32. Shulman RG, Hyder F and Rothman DL. Lactate efflux and the neuroenergetic basis of brain function. *NMR Biomed.* 2001; 14: 389-396.

33. Shulman RG, Hyder F and Rothman DL. Insights from neuroenergetics into the interpretation of functional neuroimaging: an alternative empirical model for studying the brain's support of behavior. *J Cereb Blood Flow Metab.* 2014; 34: 1721-1735.

34. Gulyas AI, Szabo GG, Ulbert I, et al. Parvalbumin-containing fast-spiking basket cells generate the field potential oscillations induced by cholinergic receptor activation in the hippocampus. *J Neurosci.* 2010; 30: 15134-15145.

35. Schlingloff D, Kali S, Freund TF, et al. Mechanisms of sharp wave initiation and ripple generation. *J Neurosci.* 2014; 34: 11385-11398.

36. Kann O, Huchzermeyer C, Kovacs R, et al. Gamma oscillations in the hippocampus require high complex I gene expression and strong functional performance of mitochondria. *Brain.* 2011; 134: 345-358.

37. Schneider J, Berndt N, Papageorgiou IE, et al. Local oxygen homeostasis during various neuronal network activity states in the mouse hippocampus. *J Cereb Blood Flow Metab.* 2019; 39: 859-873.

38. Buzsaki G. Hippocampal sharp wave-ripple: A cognitive biomarker for episodic memory and planning. *Hippocampus.* 2015; 25: 1073-1188.

39. Colgin LL. Rhythms of the hippocampal network. *Nat Rev Neurosci.* 2016; 17: 239-249.

40. Kann O, Papageorgiou IE and Draguhn A. Highly energized inhibitory interneurons are a central element for information processing in cortical networks. *J Cereb Blood Flow Metab.* 2014; 34: 1270-1282.

41. Iwasato T, Datwani A, Wolf AM, et al. Cortex-restricted disruption of NMDAR1 impairs neuronal patterns in the barrel cortex. *Nature.* 2000; 406: 726-731.

42. Raymond CS and Soriano P. ROSA26Flpo deleter mice promote efficient inversion of conditional gene traps in vivo. *Genesis.* 2010; 48: 603-606.

43. Zhang SJ, Steijaert MN, Lau D, et al. Decoding NMDA receptor signaling: identification of genomic programs specifying neuronal survival and death. *Neuron* 2007; 53: 549-562.

44. Schneider J, Lewen A, Ta TT, et al. A reliable model for gamma oscillations in hippocampal tissue. *J. Neurosci Res.* 2015; 93: 1067-1078.

45. Ta TT, Dikmen HO, Schilling S, et al. Priming of microglia with IFN-gamma slows neuronal gamma oscillations in situ. *Proc Natl Acad Sci U S A.* 2019; 116: 4637-4642. DOI: 10.1073/pnas.1813562116.

46. Traub RD, Bibbig A, Fisahn A, et al. A model of gamma-frequency network oscillations induced in the rat CA3 region by carbachol in vitro. *Eur J Neurosci.* 2000; 12: 4093-4106.

47. Babicki S, Arndt D, Marcu A, et al. Heatmapper: web-enabled heat mapping for all. *Nucleic Acids Res.* 2016; 44: W147-153.

48. Schindelin J, Arganda-Carreras I, Frise E, et al. Fiji: an open-source platform for biological-image analysis. *Nat Methods.* 2012; 9: 676-682.

49. Behrens CJ, van den Boom LP, de Hoz L, et al. Induction of sharp wave-ripple complexes in vitro and reorganization of hippocampal networks. *Nat Neurosci.* 2005; 8: 1560-1567.

50. Bazelot M, Telenczuk MT and Miles R. Single CA3 pyramidal cells trigger sharp waves in vitro by exciting interneurones. *J Physiol.* 2016; 594: 2565-2577.

51. Hajos N and Paulsen O. Network mechanisms of gamma oscillations in the CA3 region of the hippocampus. *Neural Netw.* 2009; 22: 1113-1119.

52. Markus NM, Hasel P, Qiu J, et al. Expression of mRNA Encoding Mcu and Other Mitochondrial Calcium Regulatory Genes Depends on Cell Type, Neuronal Subtype, and Ca2+ Signaling. *PLoS One.* 2016; 11: e0148164.

53. Fellmann C and Lowe SW. Stable RNA interference rules for silencing. *Nat Cell Biol.* 2014; 16: 10-18.

54. Llorente-Folch I, Rueda CB, Amigo I, et al. Calcium-regulation of mitochondrial respiration maintains ATP homeostasis and requires ARALAR/AGC1-malate aspartate shuttle in intact cortical neurons. *J Neurosci.* 2013; 33: 13957-71, 71a.

55. Nichols M, Elustondo PA, Warford J, et al. Global ablation of the mitochondrial calcium uniporter increases glycolysis in cortical neurons subjected to energetic stressors. *J Cereb Blood Flow Metab.* 2017; 37: 3027-3041.

56. Wu Y, Rasmussen TP, Koval OM, et al. The mitochondrial uniporter controls fight or flight heart rate increases. *Nat Commun.* 2015; 6: 6081.

57. Sun T, Qiao H, Pan PY, et al. Motile axonal mitochondria contribute to the variability of presynaptic strength. *Cell Rep.* 2013; 4: 413-419.

58. Smith HL, Bourne JN, Cao G, et al. Mitochondrial support of persistent presynaptic vesicle mobilization with age-dependent synaptic growth after LTP. *Elife.* 2016; 5.

59. David G and Barrett EF. Mitochondrial Ca2+ uptake prevents desynchronization of quantal release and minimizes depletion during repetitive stimulation of mouse motor nerve terminals. *J Physiol.* 2003; 548: 425-438.

60. Kannurpatti SS. Mitochondrial calcium homeostasis: Implications for neurovascular and neurometabolic coupling. *J Cereb Blood Flow Metab.* 2017; 37: 381-395.

61. Mammucari C, Raffaello A, Vecellio Reane D, et al. Mitochondrial calcium uptake in organ physiology: from molecular mechanism to animal models. *Pflugers Arch.* 2018; 470: 1165-1179.

62. Lieberman DN and Mody I. Regulation of NMDA channel function by endogenous Ca(2+)-dependent phosphatase. *Nature.* 1994; 369: 235-239.

63. Legendre P, Rosenmund C and Westbrook GL. Inactivation of NMDA channels in cultured hippocampal neurons by intracellular calcium. *J Neurosci.* 1993; 13: 674-684.

64. Marland JR, Hasel P, Bonnycastle K, et al. Mitochondrial Calcium Uptake Modulates Synaptic Vesicle Endocytosis in Central Nerve Terminals. *J Biol Chem.* 2016; 291: 2080-2086.

65. Vaccaro V, Devine MJ, Higgs NF, et al. Miro1-dependent mitochondrial positioning drives the rescaling of presynaptic Ca2+ signals during homeostatic plasticity. *EMBO Rep.* 2017; 18: 231-240.

66. Hardingham N, Dachtler J and Fox K. The role of nitric oxide in pre-synaptic plasticity and homeostasis. *Front Cell Neurosci.* 2013; 7: 190.

67. Steinert JR, Chernova T and Forsythe ID. Nitric oxide signaling in brain function, dysfunction, and dementia. *Neuroscientist.* 2010; 16: 435-452.

68. Pickles S, Vigie P and Youle RJ. Mitophagy and Quality Control Mechanisms in Mitochondrial Maintenance. *Curr Biol.* 2018; 28: R170-R185.

69. Sun N, Youle RJ and Finkel T. The Mitochondrial Basis of Aging. *Mol Cell.* 2016; 61: 654-666.

70. Reed LJ and Yeaman SJ. Pyruvate dehydrogenase. In: Boyer PD and Krebs EG (eds) *The Enzymes*. New York: Academic Press, 1987, pp.77-93.

71. McCormack JG, Halestrap AP and Denton RM. Role of calcium ions in regulation of mammalian intramitochondrial metabolism. *Physiol Rev.* 1990; 70: 391-425.

72. Mallilankaraman K, Cardenas C, Doonan PJ, et al. MCUR1 is an essential component of mitochondrial Ca2+ uptake that regulates cellular metabolism. *Nat Cell Biol.* 2012; 14: 1336-1343.

73. Patron M, Checchetto V, Raffaello A, et al. MICU1 and MICU2 finely tune the mitochondrial Ca2+ uniporter by exerting opposite effects on MCU activity. *Mol Cell.* 2014; 53: 726-737.

Figure legends

Fig. 1. Cytoarchitecture of the hippocampus in wild type (WT) and *Mcu*-KO (KO) mice. (A) Acute hippocampal slices were stained with toluidine blue (TB) in WT and KO mice. (B) The CA3 region is shown at higher magnification. Note that the cytoarchitecture of the hippocampus is well preserved. The extracellular local field potential electrode was positioned in stratum pyramidale (strongly stained layer with densely packed neuronal somas; black arrows). (C) Immunoblot analysis of microdissected hippocampal area CA3 confirms lack of MCU protein expression in *Mcu*/*Cre*$^{+}$ mice. Blots have been cropped for conciseness. (D) Quantification of immunoblot experiments. Round symbols represent individual animals, bars represent mean, error bars indicate standard deviation. P-values are indicated in the graph and were determined by one-way ANOVA followed by Tukey's multiple comparisons test. (E) Scheme of the experimental design in mice. WT (W*t*/*Cre*$^{+}$) and *Mcu*-KO (*Mcu*/*Cre*$^{+}$) littermates were used in each experiment. Acute (ex vivo) hippocampal slices were used for electrophysiological local field potential (LFP) recordings, immunostaining or qPCR arrays to obtain various readouts. The experimental design for WT and *Mcu*-KD slice cultures of the rat was similar.

Fig. 2. Gamma oscillations in mouse acute slices. Persistent gamma oscillations were recorded in stratum pyramidale of the CA3 region in acute hippocampal slices of the mouse. (A) Sample traces of local field potential recordings and corresponding wavelet transform of gamma oscillations in wild type (blue trace) and *Mcu*-KO (magenta trace) mice. (B) Sample power spectra of gamma oscillations calculated from 5 min intervals in slices from wild type (blue) and *Mcu*-KO (magenta) mice. Power spectra in (B) correspond to gamma oscillations in (A). Gamma oscillations in hippocampal slices from wild type (WT) (n = 23, N = 6) and *Mcu*-KO (n = 20, N = 6) mice were analysed for (C) the peak of the power spectrum (Power), (D) the peak frequency (f) and (E) the full width at half maximum (FWHM). Mann-Whitney rank sum test was applied for statistical analysis and Shapiro-Wilk test for normality. Statistical significance is marked by asterisks ($P < 0.05$).

Fig. 3. Gamma oscillations in rat slice cultures. Persistent gamma oscillations were recorded in stratum pyramidale of the CA3 region in hippocampal slice cultures of the rat. (A-C) Sample traces of local field potential recordings and corresponding wavelet transform of gamma oscillations in control (A, ShLacZ) and *Mcu*-knockdown (KD) slice cultures (B, Sh1; C, Sh2). (D-F) Sample power spectra of gamma oscillations calculated from 5 min intervals in control (D) and KD slice cultures (E, Sh1; F, Sh2). Gamma

oscillations in control (ShLacZ, n = 26, N = 6) and KD slice cultures (Sh1, n = 25, N = 7; Sh2, n = 15, N = 4; Sh3, n = 25, N = 8) were analysed for (C) the peak of the power spectrum (Power), (D) the peak frequency (f) and (E) the full width at half maximum (FWHM) of the gamma power. (G-I) Mann-Whitney rank sum test was applied for statistical analysis and Shapiro-Wilk test for normality. Statistical significance is marked by asterisks ($P < 0.05$).

Fig. 4. Spiking synchronization during gamma oscillations in mouse acute slices. Persistent gamma oscillations were recorded in stratum pyramidale of the CA3 region in acute hippocampal slices of the mouse. (A) Sample traces of the local field potential (top), with 700 Hz high-pass filter (middle) and extracted multi-unit ('spiking') activity (bottom) during gamma oscillations in slices from wild type (blue traces) and *Mcu*-KO (magenta traces) mice. (B) Distribution of multi-unit intervals calculated from 5 min intervals in wild type (blue, 58380 ± 3930 events, n = 23, N = 6) and *Mcu*-KO (magenta, 61500 ± 7710 events, n = 20, N = 6) mice. Red dots denote significant differences. Note that the second peak of multi-unit intervals at 20-30 ms is absent in *Mcu*-KO (magenta). (C) Distributions of the timing of multi-unit activity relative to the negative peak of the gamma-band cycle (0 ms). Red dots denote significant differences. Note that the timing of

multi-unit activity is less precise in *Mcu*-KO mice. (D) Frequency of multi-unit activity in wild type (WT) and *Mcu*-KO mice. Mann-Whitney rank sum test (B, C) and student's t-test (D) were applied for statistical analysis and Shapiro-Wilk test for normality. Statistical significance ($P < 0.05$).

Fig. 5. Sharp wave-ripples in mouse acute slices. Spontaneously-occurring, recurrent sharp wave-ripples were recorded for 5 min in stratum pyramidale of the CA3 region in acute hippocampal slices of the mouse. (A) Sample traces of local field potential recordings and corresponding wavelet transform of single sharp wave-ripples in wild type (blue trace) and *Mcu*-KO (magenta trace) mice. Sharp wave-ripples in wild type (WT) (922 ± 183 events, n = 17, N = 6) and *Mcu*-KO (717 ± 283 events, n = 16, N = 5) mice were analysed for (B) amplitude of the sharp wave (local field potential) and (C) incidence (events/s) of sharp waves as well as (D) the frequency of ripples (RP f) and (E) the number of ripples per sharp wave (#RP/SW). Mann-Whitney rank sum test and t-test were applied for statistical analysis and Shapiro-Wilk test for normality. Statistical significance is marked by asterisks ($P < 0.05$).

Fig. 6. Gamma oscillation-mediated dephosphorylation of PDH in mouse acute slices. (A) Immunofluorescence labelling of acute mouse hippocampal slices. Anti-phospho PDH labelling, anti-total PDH labelling, and a pPDH/PDH ratio image are shown for a control slice (CTL) and for a slice that underwent 40 minutes of gamma oscillations (GAM). Both slices are from the same wild type mouse. Scale bars represent 20 µm. (B) Quantification of pPDH/PDH ratio in control slices (CTL) and slices that underwent 40 minutes of gamma oscillations (GAM). Slices from three animals were analysed for both conditions in each genotype. Round symbols represent individual animals; bars represent mean ratio. Values were normalized to average ratio in wild type control slices. (C) Quantification of gamma oscillation-mediated PDH dephosphorylation in wild type and *Mcu*-KO acute slices. Round symbols represent individual animals, horizontal lines represent mean difference between control and gamma oscillations, error bars indicate 95% CI. P value was determined by unpaired two-tailed student's t-test.

Fig. 7. Expression of genes related to glucose metabolism and mitochondria in the mouse hippocampal region CA3 and summary scheme. (A, B) Heatmaps illustrating the results of RT^2 Profiler PCR Array gene expression analyses of glucose metabolism-related (A) and mitochondria-related (B) genes. N = 5 mice per genotype. Colour scale represents log10 of

normalized expression (2^{-dCT}). (C, D) Comparison of average expression per gene in wild type versus *Mcu*-KO mice for glucose metabolism-related (C) and mitochondria-related (D) genes. Dotted lines indicate 2-fold up- or down-regulation. (E) Summary of the main findings and potential pathophysiological mechanisms triggered by loss of the neuronal MCU. The relative contributions of impaired oxidative energy metabolism and impaired intracellular Ca^{2+} homeostasis to different abnormal neuronal network rhythms as well as the disturbances of higher brain functions need to be investigated in future studies. For details, see main text.

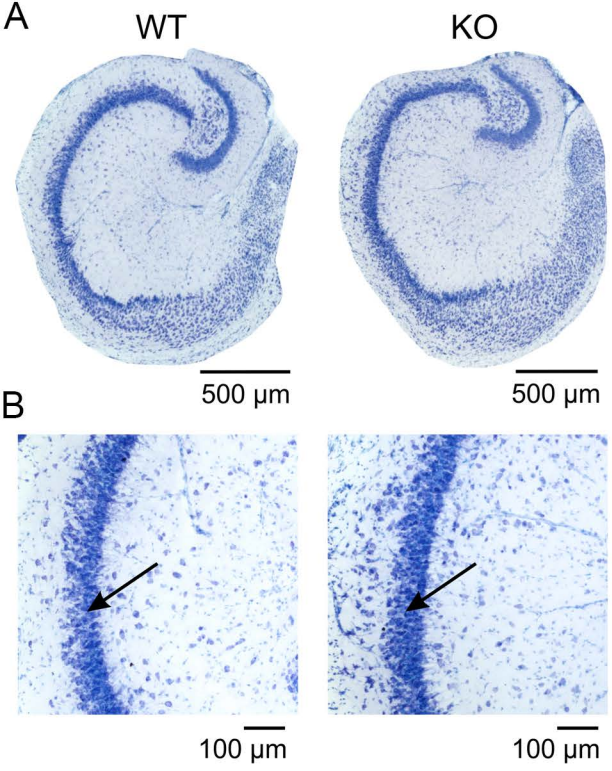

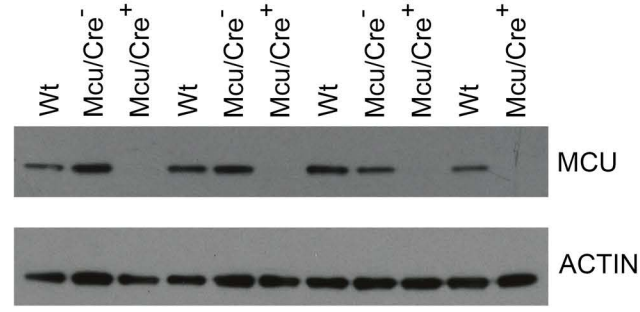

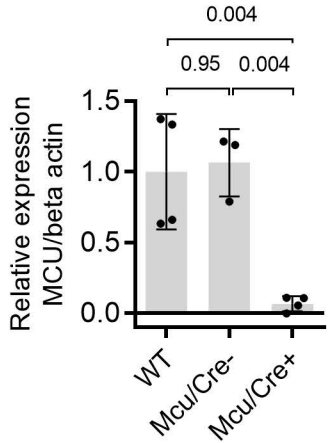

E

Set 1

WT and KO littermates → Acute hippocampal slices → LFP recordings; Immunostaining

Set 2

WT and KO littermates → Acute hippocampal slices → LFP recordings; qPCR arrays

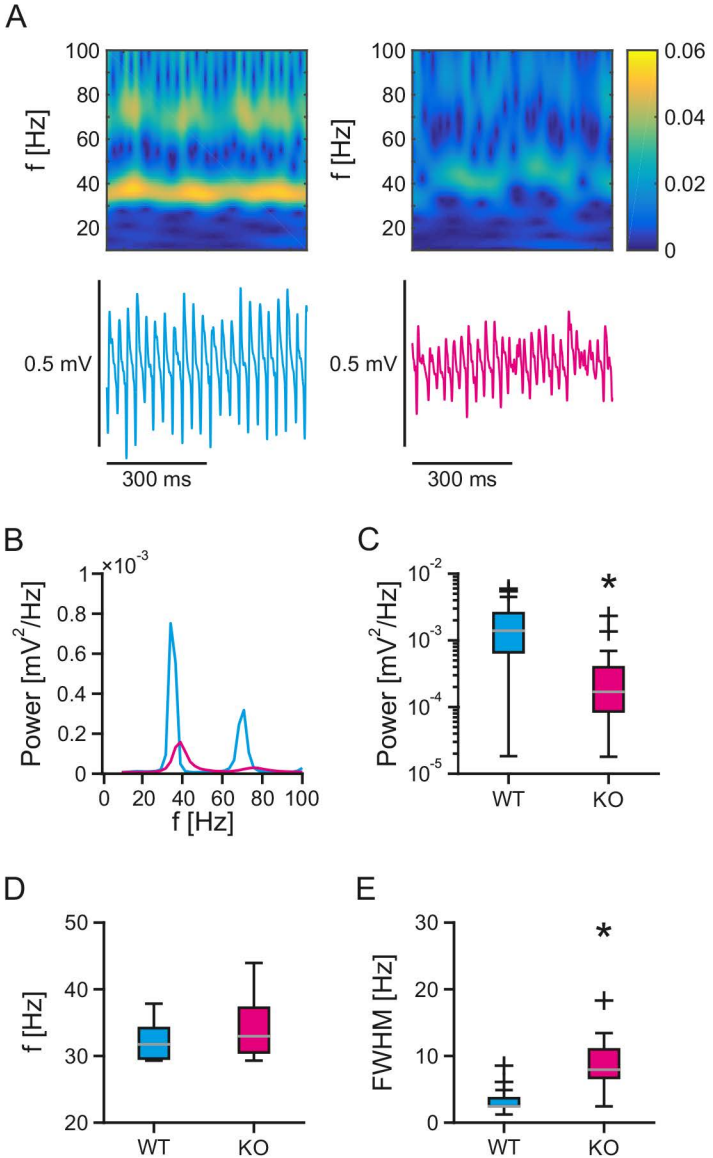
A
f [Hz]
100
80
60
40
20
0.06
0.04
0.02
0
0.5 mV
300 ms
B
Power [mV²/Hz]
×10⁻³
1
0.8
0.6
0.4
0.2
0
0 20 40 60 80 100
f [Hz]
C
Power [mV²/Hz]
10⁻²
10⁻³
10⁻⁴
10⁻⁵
WT
KO
*
D
f [Hz]
50
40
30
20
WT
KO
E
FWHM [Hz]
30
20
10
0
WT
KO
*

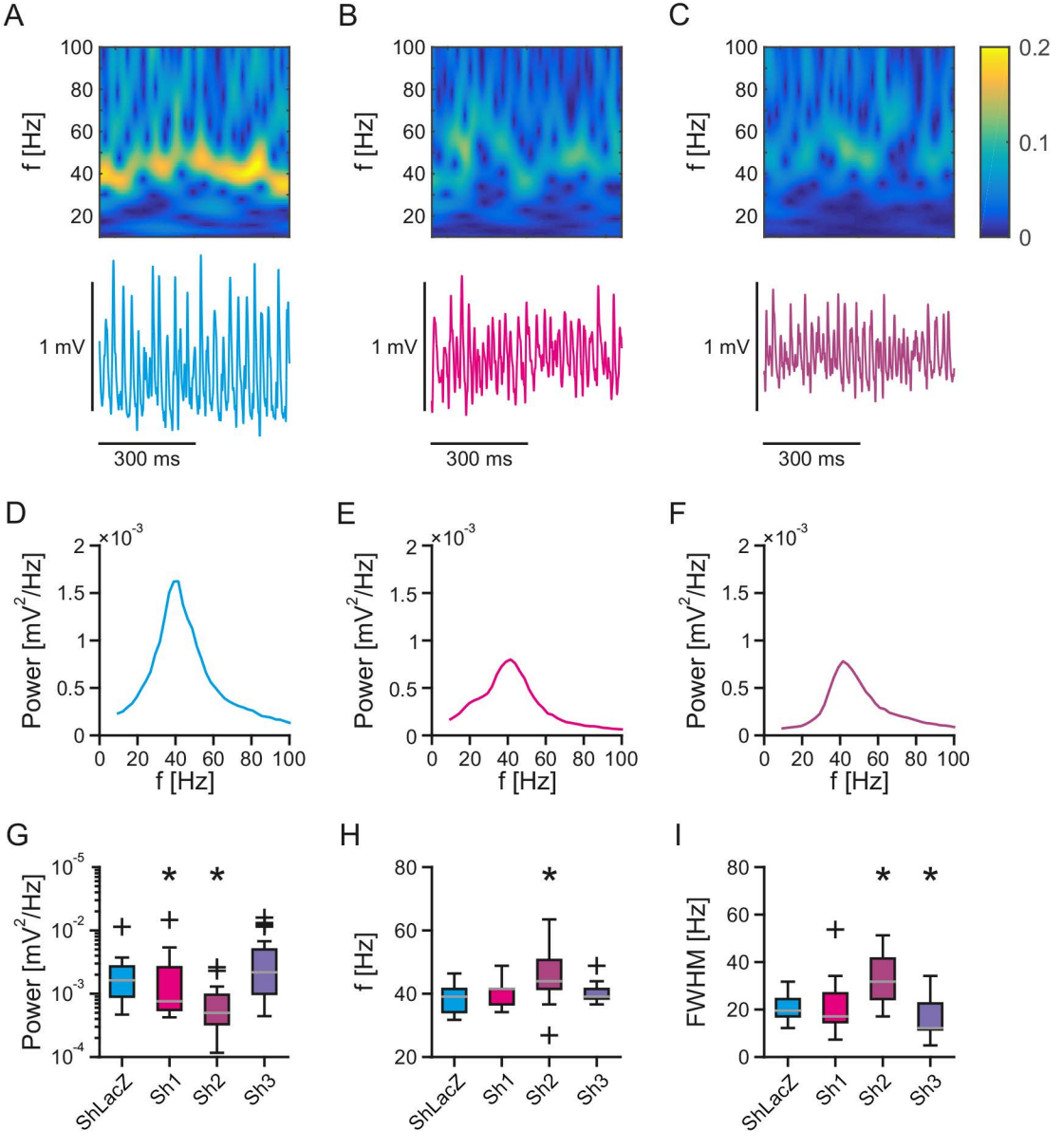
A
B
C
f [Hz]
100
80
60
40
20
0.2
0.1
0
1 mV
300 ms
D
E
F
Power [mV²/Hz]
×10⁻³
2
1.5
1
0.5
0
0 20 40 60 80 100
f [Hz]
G
H
I
Power [mV²/Hz]
10⁻⁵
10⁻²
10⁻³
10⁻⁴
f [Hz]
FWHM [Hz]
*
+
ShLacZ
Sh1
Sh2
Sh3

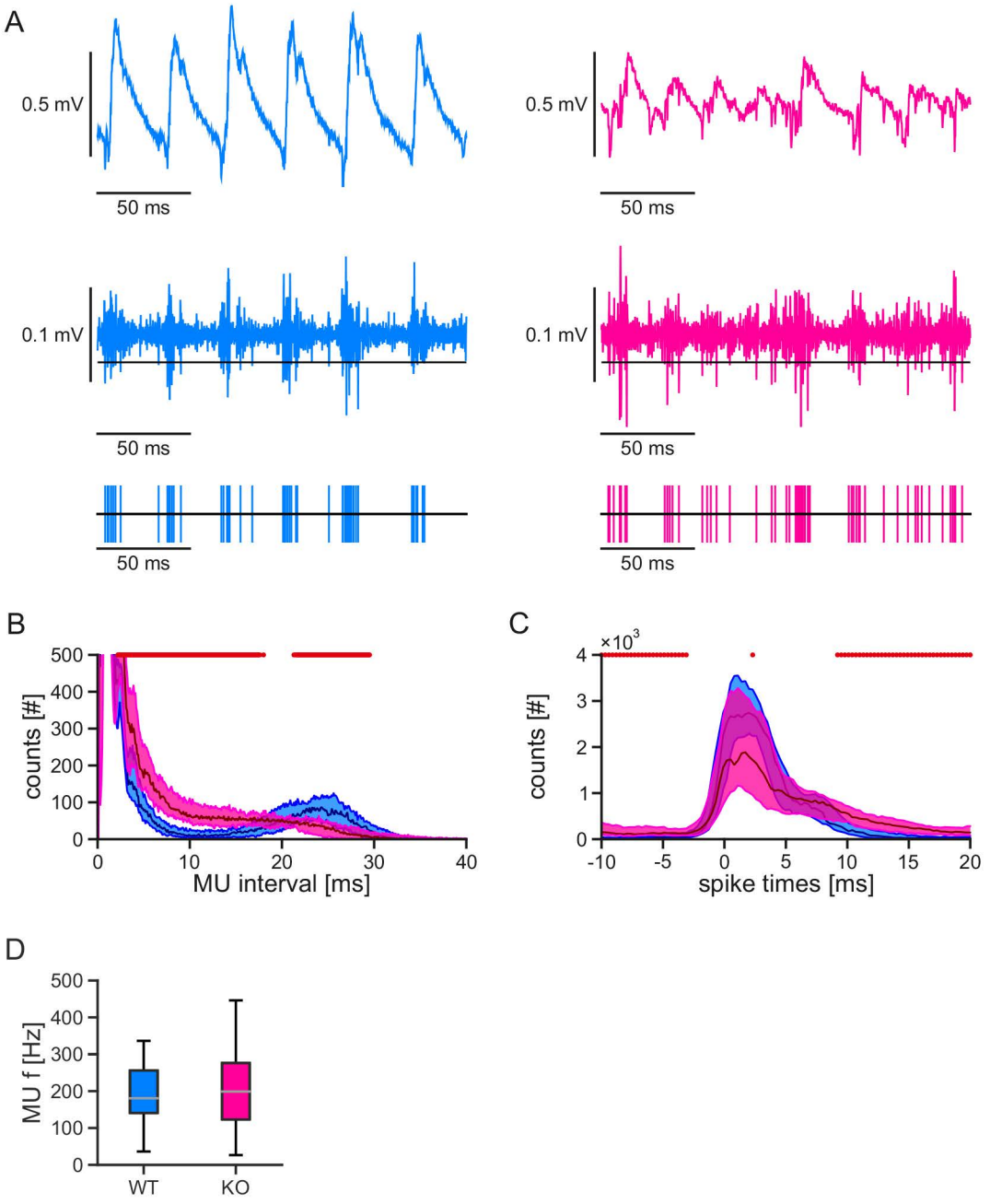
A
0.5 mV
50 ms
0.1 mV
50 ms
50 ms
0.5 mV
50 ms
0.1 mV
50 ms
50 ms
B
counts [#]
MU interval [ms]
C
×10^3
counts [#]
spike times [ms]
D
MU f [Hz]
WT
KO

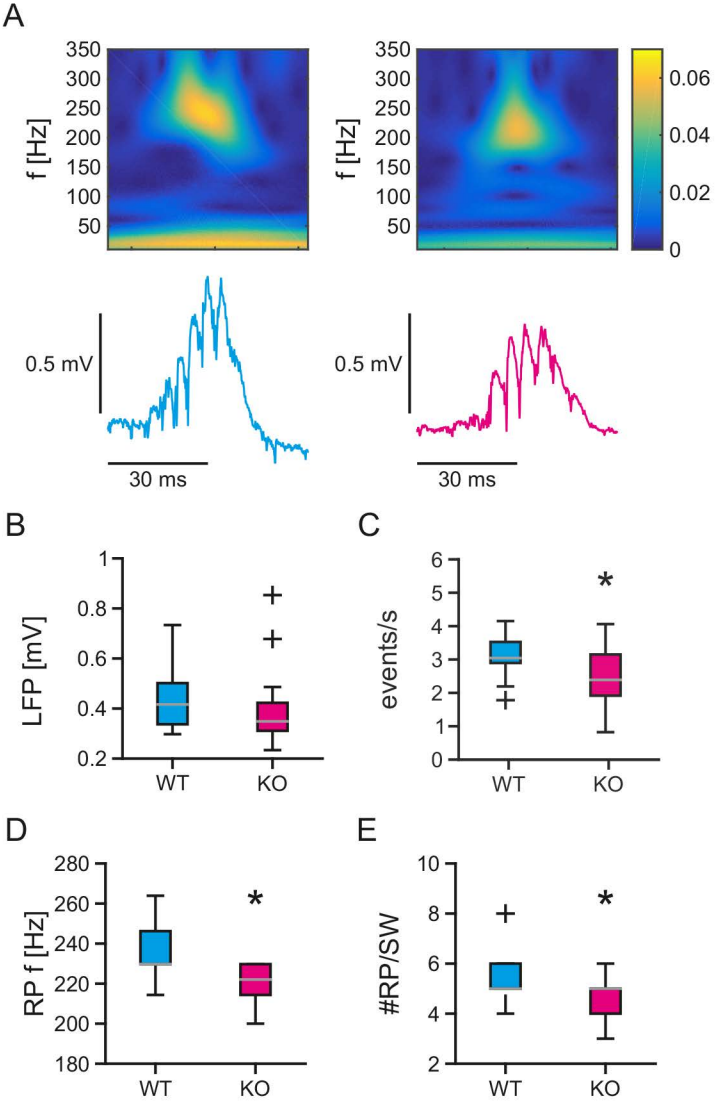
A
f [Hz]
350
300
250
200
150
100
50
0.06
0.04
0.02
0
0.5 mV
30 ms
B
LFP [mV]
1
0.8
0.6
0.4
0.2
WT
KO
C
events/s
6
5
4
3
2
1
0
*
D
RP f [Hz]
280
260
240
220
200
180
E
#RP/SW
10
8
6
4
2

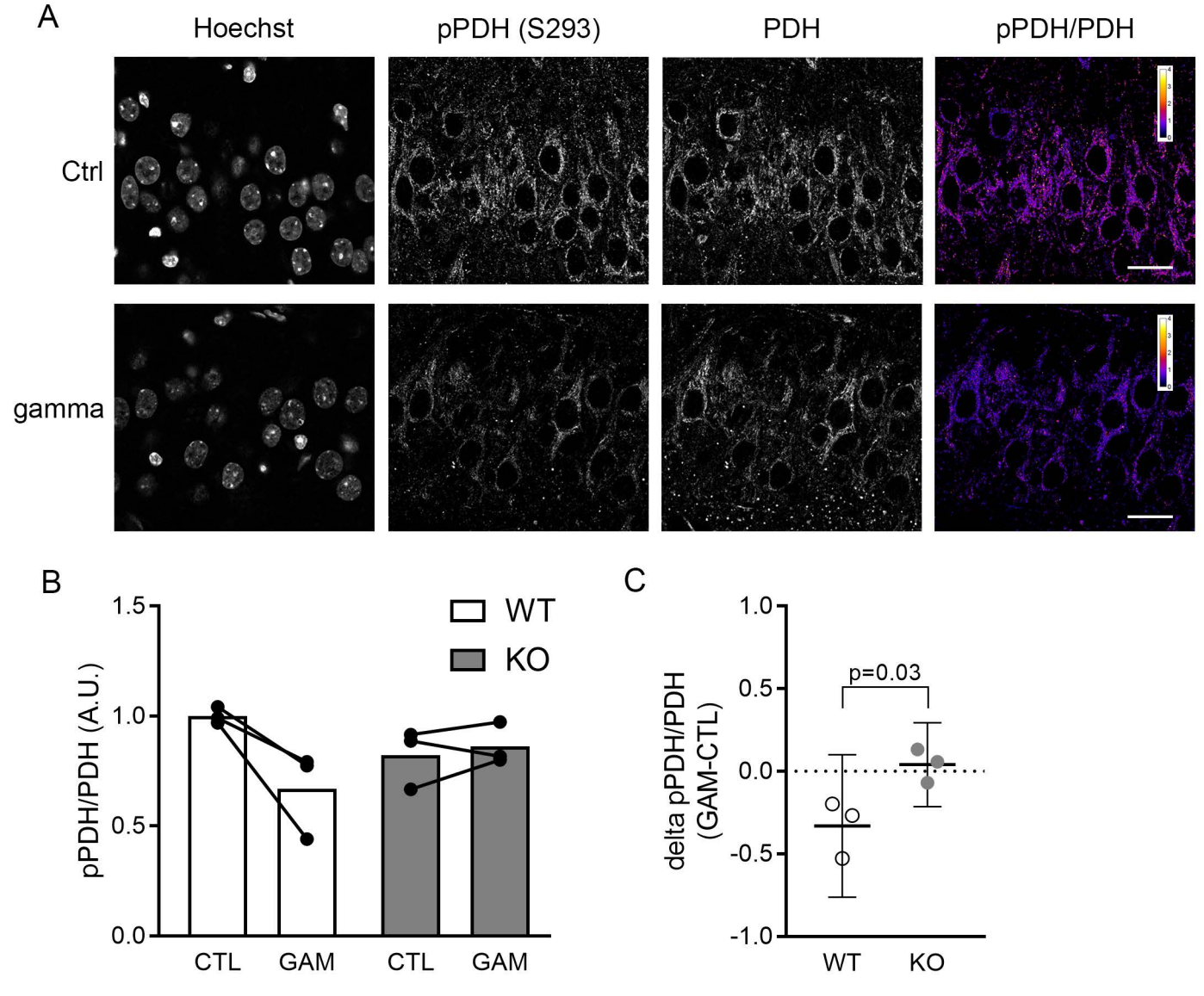
A
Hoechst
pPDH (S293)
PDH
pPDH/PDH
Ctrl
gamma
B
pPDH/PDH (A.U.)
1.5
1.0
0.5
0.0
WT
KO
CTL
GAM
CTL
GAM
C
delta pPDH/PDH (GAM-CTL)
1.0
0.5
0.0
-0.5
-1.0
p=0.03
WT
KO

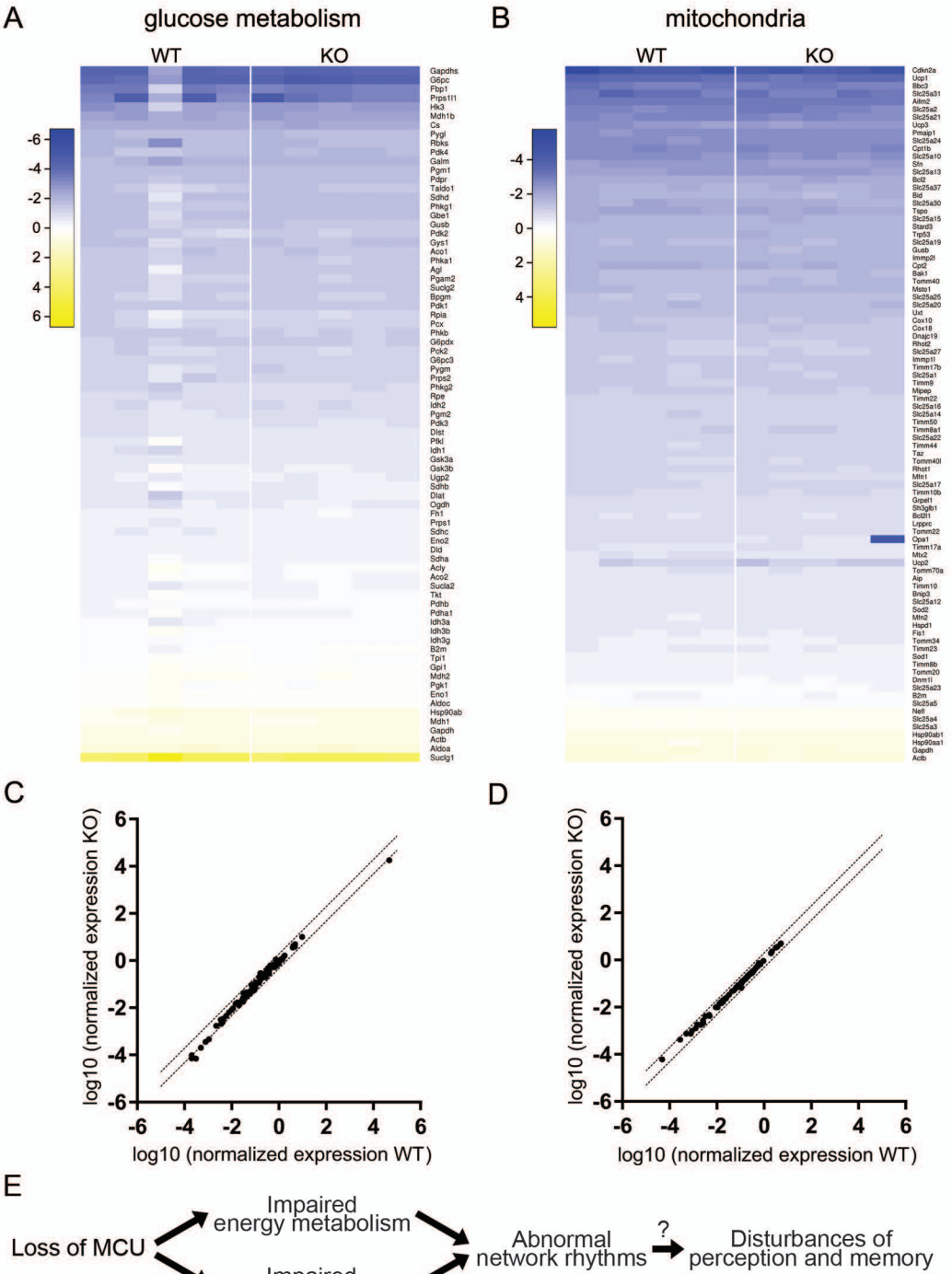
A
glucose metabolism
WT
KO
B
mitochondria
WT
KO
C
log10 (normalized expression KO)
log10 (normalized expression WT)
D
log10 (normalized expression KO)
log10 (normalized expression WT)
E
Loss of MCU
Impaired energy metabolism
Impaired Ca2+-homeostasis
Abnormal network rhythms
?
Disturbances of perception and memory